Analytical Biochemistry 498 (2016) 1–7

Contents lists available at ScienceDirect

Analytical Biochemistry

journal homepage: www.elsevier.com/locate/yabio

Design and development of high bioluminescent resonance energy transfer efficiency hybrid-imaging constructs

Manoj Kumar [a, b], Letícia Kovalski [a], David Broyles [a], Eric A. Hunt [a], Pirouz Daftarian [a], Emre Dikici [a], Sylvia Daunert [a], Sapna K. Deo [a, *]

[a] Department of Biochemistry and Molecular Biology, Miller School of Medicine, University of Miami, Miami, FL 33136, USA
[b] Indian Institute of Technology (BHU), Department of Chemical Engineering and School of Biomedical Engineering, Varanasi, UP 221005, India

ARTICLE INFO

Article history:
Received 1 April 2015
Received in revised form
6 November 2015
Accepted 23 November 2015
Available online 7 January 2016

Keywords:
Bioluminescence
Bioluminescence resonance energy transfer
Quantum dots
Renilla luciferase
Imaging construct

ABSTRACT

Here we describe the design and construction of an imaging construct with high bioluminescent resonance energy transfer (BRET) efficiency that is composed of multiple quantum dots (QDs; $\lambda_{em} = 655$ nm) self-assembled onto a bioluminescent protein, *Renilla* luciferase (Rluc). This is facilitated by the streptavidin–biotin interaction, allowing the facile formation of a hybrid-imaging construct (HIC) comprising up to six QDs (acceptor) grafted onto a light-emitting Rluc (donor) core. The resulting assembly of multiple acceptors surrounding a donor permits this construct to exhibit high resonance energy transfer efficiency (~64.8%). The HIC was characterized using fluorescence excitation anisotropy measurements and high-resolution transmission electron microscopy. To demonstrate the application of our construct, a generation-5 (G5) polyamidoamine dendrimer (PAMAM) nanocarrier was loaded with our HIC for in vitro and in vivo imaging. We envision that this design of multiple acceptors and bioluminescent donor will lead to the development of new BRET-based systems useful in sensing, imaging, and other bioanalytical applications.

Extensive effort has been invested in the design, development, characterization, and application of efficient light-emitting constructs using energy transfer [1]. Such optically active constructs have a strong impact on many scientific fields such as in the development of sensitive and selective biosensors [2–6], molecular medicine imaging [7–10], and others [1,6,7,11–16]. Part of this motivation for advanced resonance energy transfer (RET) platforms arises from the difficulty in tuning self-illuminating imaging constructs such as bioluminescent proteins for red-shifted emission. Although the Gambhir laboratory has made important advances in this regard [17], the limited (66-nm) bandwidth of these *Renilla* luciferase mutants combined with their intrinsically broad emission leaves little opportunity for multiplexing. However, the increased complexity of fabrication for RET systems naturally dictates the need for facile, rapid, and reproducible synthesis to truly revolutionize the application of these constructs. This can be achieved by developing methodologies in which individual reagent components are modified in such a way as to support self-assembly [18] of the desired light-emitting constructs. These light-emitting constructs often use fluorescent resonance energy transfer (FRET) [3,19] or bioluminescent resonance energy transfer (BRET) [4,20–23] mechanisms.

The optimization of a resonance energy transfer system involves proper matching of donor-to-acceptor energy levels in order to exhibit the desired emission characteristics. For example, to obtain high quantum yield and a high signal-to-noise ratio of the emitted energy, a large molar extinction coefficient, narrow emission, and good photostability from the acceptor are desired. Many commercially available organic dyes fulfill some of these requirements; however, they can be either sensitive to photobleaching or unstable under different pH values, exhibit small Stokes shifts, have narrow excitation and broad emission peaks, or have small molar extinction coefficients. Recent developments in the synthesis of colloidal

Abbreviations used: RET, resonance energy transfer; FRET, fluorescent resonance energy transfer; BRET, bioluminescent resonance energy transfer; QD, quantum dot; UV–Vis, ultraviolet–visible; CL, chemiluminescent; Rluc, Renilla luciferase; IVIS, In Vitro Imaging System; HIC, hybrid-imaging construct; QDSV, streptavidin-modified QDs; bRluc, biotin-modified Rluc; biotin-NHS ester, biotin-N-hydroxysuccinimide ester; G5-PAMAM, generation-5 polyamidoamine dendrimer; FBS, fetal bovine serum; EDTA, ethylenediaminetetraacetic acid; HR–TEM, high-resolution transmission electron microscopy; HIC-D, HIC encapsulated with G5-PAMAM dendrimer; PDD, peptide G5-PAMAM dendrimer; PBS, phosphate-buffered saline.

* Corresponding author.
E-mail address: sdeo@med.miami.edu (S.K. Deo).

http://dx.doi.org/10.1016/j.ab.2015.11.028
0003-2697/

semiconducting nanoparticles have expanded their use in various optically demanding applications such as FRET, BRET, and chemiluminescent resonance energy transfer (CRET) [20]. These luminescent quantum dots (QDs) have good photostability and high fluorescence quantum yield. Currently, commercially available QDs such as the widely used CdSe/ZnS and CdSe/CdTe, or the biocompatible InP/ZnS dots, can cover the full optical absorption spectrum while maintaining a narrow emission band (~45–50 nm) for application in sensing, imaging, and energy production (dye-sensitized solar cells or solar concentrators) [24]. Their broad ultraviolet–visible (UV–Vis) excitation band allows simultaneous excitation of multiple color QDs, allowing them to be considered as universal resonant energy donors. At the same time, their narrow emission allows for highly selective energy transfer to the appropriate fluorophore. However, the application of QD-based, UV–Vis FRET systems is limited in biological medium (tissues, organs, or cells) due to high biological attenuation of these wavelengths [15,21,22,25], which results in weak and diffuse emission. In addition, the use of high-power sources for QD excitation is required in order to penetrate the tissue. Consequently, high-energy excitation results in photobleaching of the acceptor dye and significant background from the biological media (autofluorescence). All of these factors are detrimental to the observed signal-to-noise (S/N) ratio. In addition, the broad emission of most fluorophores restricts the degree of multiplexing available for sensing or imaging constructs [26]. Although the broad UV–Vis absorption band of QDs makes them suitable as energy donors, their application as energy acceptors remained relatively limited until recently [4,27] and is mainly limited to sensing applications [28,29]. Du and coworkers [20] reported the design of QD-decorated chemiluminescent (CL) nanocapsules employing vinyl-encapsulated horseradish peroxidase conjugated to QDs. CL was generated using hydrogen peroxide and *p*-iodophenol as substrates. However, in vivo imaging using this construct was not shown, possibly due to the weak CL signal and complexity of the system. Here we describe a construct using QDs as the energy acceptor from a bioluminescence-based excitation energy source [21,23] placed in close proximity to the QDs.

Renilla luciferase (Rluc) is a bioluminescent protein that generates light as a result of a chemical reaction with its “luciferin” substrate, coelenterazine. This radiative energy can be used for direct imaging or as the excitation source for organic dyes or QDs. The emission spectrum of coelenteramide overlaps with the QD absorption spectra to provide resonance energy transfer that results in near-infrared QD emission for efficient biological matrix penetration (mm–cm) [7] and higher optical imaging sensitivity. A variation of this concept was previously demonstrated using self-illuminating QDs [21]. In this work, multiple Rluc (donors) were linked to a single QD (acceptor) through a zero-length cross-linker. This multiple donor–single acceptor method using a short Rluc–QD separation distance resulted in 56% BRET efficiency. The optimized construct was used for bioimaging using the In Vivo Imaging System (IVIS). This novel design allowed tissue imaging without the need for an exogenous excitation source. However, this application of multiple donors around a single acceptor required time-consuming conjugation chemistry.

In the current work, a new design is presented for a hybrid-imaging construct (HIC) based on the BRET principle that demonstrates high efficiency, self-assembly, and near-infrared illumination. The design is based on facile streptavidin–biotin chemistry, which enables a multiple acceptor–donor construct for superior BRET-based imaging. The HIC incorporates a network of streptavidin-modified QDs (QDSV) surrounding a biotin-modified Rluc (bRluc). A multiple acceptor–single donor configuration has not been demonstrated previously in a BRET study. Our system capitalizes on the fact that an increase in FRET efficiency was observed when multiple energy acceptors surrounded a single energy donor in several studies [3,5,6,30–32]. Due to the high quantum yield, large molar extinction coefficient, and broad absorption band [33] of the QD acceptors, a well-resolved, red-shifted, and stable emission is obtained. Bioluminescence emission from the donor (bRluc) in combination with the high excitation efficiency of the multiple QD acceptors results in low signal scattering and superior image quality for in vitro and in vivo imaging applications. The major advancement of this work comprises the ability to assemble the complete HIC using a facile technique that does not require complicated conjugation while exceeding the BRET efficiency of similar platforms that require significantly more synthetic manipulation. In addition, this is the first report of a BRET-based single donor–multiple acceptor construct, and this design was found to exceed the BRET efficiency observed in previously reported work.

Materials and methods

Materials

All purchased chemicals were used without further purification. Streptavidin-modified QDs emitting at 655 nm (QDSV) were purchased from Invitrogen (Carlsbad, CA, USA). Biotin-*N*-hydroxysuccinimide ester (biotin-NHS ester, 98% HPLC purified) and *N*-(3-dimethylaminopropyl)-*N*′-ethylcarbodiimide hydrochloride (EDC), ethylenediamine core generation-5 polyamidoamine dendrimer (G5-PAMAM), and fetal bovine serum (FBS) were purchased from Sigma–Aldrich. Targeted peptide (AKXVAAWTLKAAAZC)–G5 dendrimer conjugate was purchased from 21st Century Biochemicals. 96-Well microtiter plates with nonbinding surface were purchased from Corning (Corning, NY, USA). Microcon YM-100 (100 kDa MWCO) spin columns were purchased from Millipore (Billerica, MA, USA). Native coelenterazine was obtained from Prolume (Pinetop, AZ, USA). Zeba desalting spin columns (7 kDa MWCO), monobasic sodium phosphate anhydrous, and dibasic sodium phosphate heptahydrate were purchased from Thermo Fischer Scientific (Rockford, IL, USA). Dulbecco's modified Eagle's medium/Ham's F12 50:50 mix, 1% antibiotic–antimycotic solution, and trypsin–EDTA (ethylenediaminetetraacetic acid) were purchased from Cellgro (Manassas, VA, USA).

Renilla luciferase–biotin conjugation

Rluc was expressed and purified using methods developed in our laboratory [4]. Biotin-NHS ester was used to conjugate biotin to the free amine groups on Rluc. In a typical reaction, 1.1 nmol of Rluc was reacted with 11 nmol of biotin-NHS ester in 200 μl of 100 mM phosphate buffer (pH 8.0). The reaction was allowed to continue for 15 min prior to buffer exchange through Zeba desalting spin columns (7 kDa MWCO). The bRluc conjugates were buffer exchanged to 100 mM phosphate buffer (pH 7.0) and kept at 4 °C until further use. The bioluminescence emission of bRluc was measured and compared with Rluc, showing no significant effect of conjugation on the bioluminescence of Rluc.

Bioluminescence measurements

To synthesize self-assembled HIC, 1 pmol of bRluc was added to 100 mM phosphate buffer (pH 7.0) in a 96-well microtiter plate, followed by the incremental addition of QDSV from a 2-μM stock solution. This mixture was incubated for 15 min at 25 °C. To the final mixture volume of 150 μl, 50 μl of a 2-μg/ml solution of coelenterazine was injected, and luminescence was recorded using 486 ± 10 and 680 ± 10 nm emission filters with bioluminescent

measurements on a Victor X Light luminometer (PerkinElmer). In addition, the spectral output of the HIC was recorded under similar conditions using a Labsystem Luminoskan Ascent Microplate Reader (Thermo Labsystems, Franklin, MA, USA) with a water-cooled charge-coupled device (CCD).

Given the potential for extrinsic signal losses in vivo, we evaluated the possibility of further signal loss due to the inner filter effect using an Agilent UV–Vis spectrophotometer. Briefly, 200 μl of the HIC complex was drawn from each well of the 96-well microtiter plates following completion of the BRET characterization, and the transmittance and absorbance of the solution were measured. A solution of 100 mM phosphate buffer (pH 7.0) was used as a blank.

Fluorescence excitation anisotropy measurements

Fluorescence excitation anisotropy measurements were carried out using a Quantum Master 40 fluorescence spectrophotometer (Photon Technology International, Birmingham, NJ, USA). The excitation spectrum of coelenteramide was achieved through an excitation polarizer (385 nm), whereas emission was collected through a 500-nm emission polarizer using a 4-nm slit opening. Fluorescence excitation anisotropy data were collected for each sample at a rate of 0.1 points/s for 200 s. Briefly, 1 pmol of bRluc was added to 100 μl of 100 mM phosphate buffer (pH 7.0), followed by the addition of 0.5 μg/ml coelenterazine. Fluorescence excitation anisotropy was recorded after a 5-min incubation to allow for the conversion of coelenterazine to coelenteramide. To this mixture, a stock solution of 0.5 μM QDSV was added in increments of 1–2 μl until reaching 8 pmol. After each QDSV addition, fluorescence excitation anisotropy measurements were recorded at 15-min intervals.

HR–TEM analysis

For high-resolution transmission electron microscopy (HR–TEM) analysis, 1 μl of either a 6-μM QDSV stock solution or a 6-μM HIC solution was drop-casted on a copper grid and allowed to dry. Samples were analyzed using a high-resolution JEOL transmission electron microscope (JEM-2100) equipped with a LaB6 filament operating at 200 kV.

Synthesis of HIC–PAMAM dendrimer complex

For imaging analyses, the HIC was encapsulated with G5-PAMAM dendrimer (HIC-D). For this, a solution containing 6 pmol of QDSV was added to 1 pmol of bRluc and incubated for 15 min at room temperature. Subsequently, 10 pmol of a G5-PAMAM solution was added [34]. The control consisted of 1 pmol of bRluc and 10 pmol of G5-PAMAM in the absence of QDSV. Dendrimer encapsulation of the construct was performed overnight and used for imaging the following day. For in vivo imaging, the HIC complex was encapsulated with targeting peptide G5-PAMAM dendrimer (PDD) to create HIC–PDD using a similar procedure. A control conjugate of bRluc–PDD was also prepared.

In vitro imaging

ARPE-19 cells were cultured in Dulbecco's modified Eagle's medium/Ham's F12 50:50 mix supplemented with 10% heat-inactivated FBS and 1% antibiotic–antimycotic solution. Cells were incubated at 37 °C in 98% humidified air containing 5% CO_2. For HIC-D imaging, cells were grown to 90% confluence, washed with phosphate-buffered saline (PBS), and detached with 0.25% trypsin–EDTA. Cells were then counted and resuspended at a density of 2×10^6 cells/ml in Opti-MEM Reduced Serum Medium. Aliquots (500 μl) containing 1×10^6 cells were treated with the complexes (9.96 pmol) and incubated at 37 °C for 30 min. The cell–complex mixture was centrifuged for 5 min at 500 *g*, washed with 500 μl of PBS twice, divided into two aliquots of 250 μl, and centrifuged for 5 min at 700 *g*. Prior to imaging, cells were resuspended by pipetting, followed by the addition of 10 μg coelenterazine. The images were acquired with an IVIS Spectra (Caliper Life Science) in the auto mode using 660 ± 20 and 500 ± 20 nm emission filters, and the acquired images were analyzed using Living Image 4.2 software (available free of cost at http://www.caliperls.com/support/software-downloads.htm).

In vitro mice imaging

Two C57BL/6 mice were injected subcutaneously with HIC–PDD and bRluc–PDD as imaging construct and control, respectively. After 4 h, 100 μl of 100 ng/μl coelenterazine was administered by intraperitoneal (IP) injection, and the mice were imaged for 60 s. Prior to imaging, the peritoneum of mice was incised dorsally and imaged by IVIS. The emission from HIC–PDD and bRluc–PDD was collected using a 660 ± 20 nm filter. The obtained images were analyzed using Live Imaging 4.2 software (available at the IVIS website) http://www.perkinelmer.com/Catalog/Product/ID/IVISSPE.

Results and discussion

The general scheme for the HIC (Fig. 1) relies on multiple energy acceptors surrounding a central bioluminescent donor core for efficient energy transfer. The initial optical characterization of BRET in the HIC demonstrated high-intensity emission at 655 nm from QDs with a concurrent decrease in the emission from Rluc (Fig. 2A). The inner filter effect, or a decreasing linearity between the HIC concentration and fluorescent output due to reabsorption of the signal at higher concentrations [32], was evaluated for any effect on the BRET efficiency. Using aliquots drawn from the titration experiment, we were able to show that signal reabsorption had a negligible contribution toward overall BRET signal (data not presented). In Fig. 2A, "I_{nc}" represents the normalized intensity following correction for the inner filter effect [32]. As shown in Fig. 2B, optimization of the QDSV:bRluc ratio led to a BRET efficiency maximum at 6 pmol of QDSV when plotted against a bRluc concentration of 1 pmol. A reproducible BRET efficiency curve was obtained with different batches of HIC construct. BRET efficiency of the system was calculated using Eq. (1) [32]:

$$E = 1 - (I_{DA}/I_D) \times 100\%, \quad (1)$$

where I_D and I_{DA} represent the emission intensity of the donor in the absence and presence of acceptor, respectively. As shown in Fig. 2B, BRET efficiency increased to a maximum of 64.8% at a QDSV:bRluc ratio of 6 and remained unchanged on further increases in QDSV concentration.

A certain degree of nonspecific interaction between Rluc and QDs can be expected. However, the strong streptavidin–biotin affinity and the reproducible BRET signal saturation ratio strongly indicated the self-assembly of multiple QDSV and bRluc. Although it is possible that these HIC constructs could lead to mixtures of ratio from 1:1 to 1:6 or higher, the higher ratio does not affect BRET efficiency. The use of a 1:6 ratio between bRluc and QDSV resulted in reproducible BRET efficiency for different batches, indicating that a majority of complexes follow this configuration. Furthermore, to ensure that the formation of the HIC was complete, steady-state fluorescence excitation anisotropy experiments were performed using the fluorescence excitation of coelenteramide. Coelenteramide is produced from the

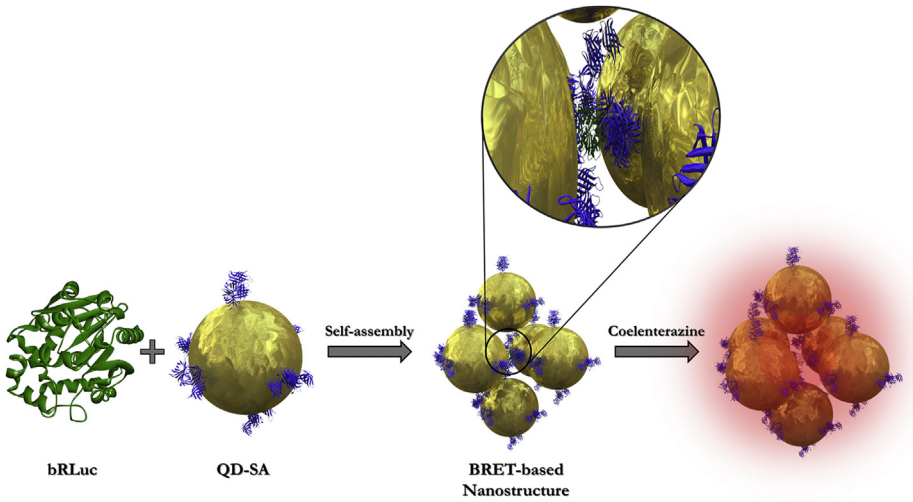

Fig.1. A simplified schematic representation of the imaging construct synthesis. Although enlarged slightly to show detail, the diameter of Rluc measures approximately half the length of the cylindrical quantum dots, with axial crystallographic dimensions of 8.92 × 5.1 × 7.4 nm for Rluc (PDB ID: 2PSJ) [35] versus approximately 20 nm (Invitrogen) for the streptavidin-functionalized nanocrystals. Biotinylated Rluc (1 pmol) mixed with streptavidin-modified QDs (6 pmol) results in formation of the HIC.

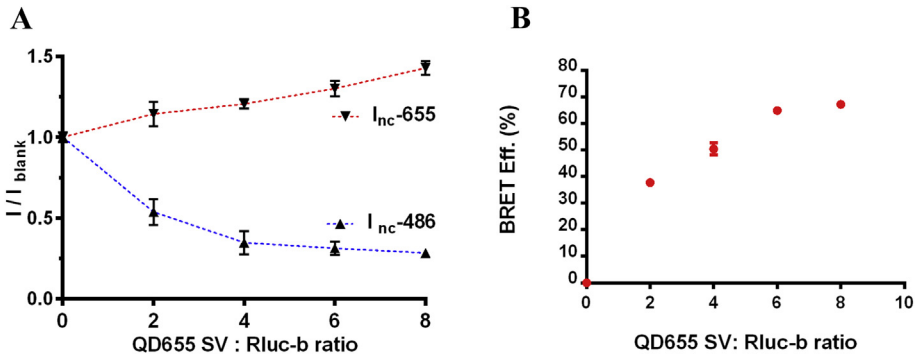

Fig.2. Optical characteristics of the hybrid-imaging construct (HIC) showing the normalized intensity of the QD (red curve, upper) and Rluc (blue curve, lower) emissions for increasing QDSV:bRluc ratios (A) and variation in BRET efficiency with respect to an increase in QDSV:bRluc ratio (B). (For interpretation of the references to colour in this figure legend, the reader is referred to the web version of this article.)

oxidation of coelenterazine within the Rluc pocket [36,37] and remains bound to Rluc after oxidation due to its higher binding affinity [36]. The fluorescence properties of coelenteramide (Fig. 3A) provided a means to correlate QDSV binding to bRluc and fluorescence excitation anisotropy changes (Fig. 3B). Anisotropy (r) can be loosely defined by the Perrin equation as the ratio of the maximum polarization exhibited by a static molecule to the loss of polarization due to rotational diffusion. When comparing anisotropy within the same system, fluorescence lifetime and maximum polarization are constant, so only a change in rotational diffusion will perturb the system and provide an anisotropy change. As QDSV became immobilized on the surface of bRluc, the rotational diffusion was expected to decrease incrementally until all binding sites were occupied or further binding of QDSV was sterically hindered. In either case, fluorescence excitation anisotropy was expected to increase

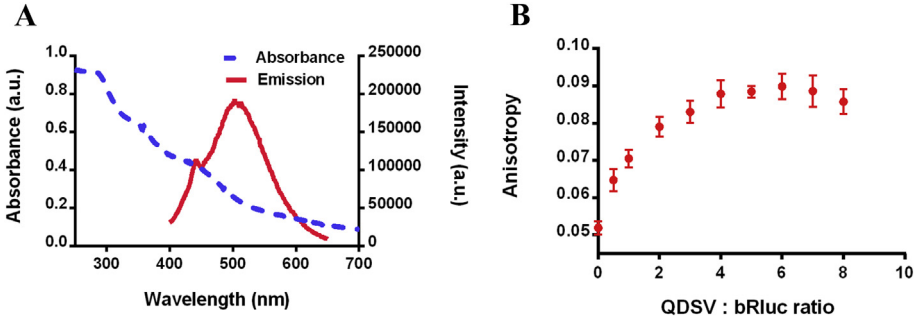

Fig.3. Characterization of multiple QDSV around bRluc using anisotropy experiments: (A) absorbance (—) and emission (—) of coelenteramide; (B) anisotropy change on increasing the ratio of QDSV:bRluc.

toward a limit defined by the maximum coordination of the HIC. It was observed that the anisotropy value for bRluc without QDSV was on the order of 0.05, which resulted from the high internal flexibility and rapid rotational diffusion of the protein. On subsequent addition of QDSV, the anisotropy values increased from 0.05 to approximately 0.09, likely as a result of decreases in both intrinsic flexibility and rotational diffusion. Anisotropy of the system reached its maximum at a QDSV:bRluc ratio of approximately 6 and remained invariant to further ratio increases. This corroborated the interaction of multiple QDSV around a single bRluc with a maximum ratio of 1:6. Based on steady-state fluorescence excitation anisotropy, the fraction of QDSV attached to bRluc was calculated using Eq. (2) [32]:

$$f_b = (r - r_F)/(r_B - r_F), \quad (2)$$

where r is the measured anisotropy, r_F and r_B are the anisotropy of free and bound bRluc, respectively, and f_b represents the fraction of bound bRluc. Based on this equation, the average f_b was calculated to be approximately 80.6%.

We also performed HR–TEM analysis using our HIC complex (Fig. 4). The TEM image shows the formation of HIC ranging from 1:3 to 1:6 ratio of bRluc:QDSV. The utility of the HIC prepared in this study was demonstrated for in vivo imaging applications. First, we verified that the HIC could be successfully transported into an in vitro model tissue. For this study, we chose G5-PAMAM dendrimer nanocarrier for transport of the HIC into cells and tissue because the uptake via endocytosis of G5-PAMAM dendrimer-conjugated cargo has been well established in the literature. The possibility of nonspecific adsorption of the HIC complex on cell surface was reduced by performing several wash steps. G5-PAMAM dendrimer is a tree-like polymeric structure that terminates in primary amines, allowing for efficient complexation of DNA, proteins, and drugs through ionic interactions. Daftarian and coworkers [34] demonstrated that G5-PAMAM–DNA complexes (>200 nm in size) efficiently crossed cell membranes. Thus, we relied on the same platform for transfection [34] of the HIC complex into human retinal pigment epithelium (ARPE-19) cells [38]. Following complexation with G5-PAMAM, no change in the optical properties of the HIC was observed, likely as a result of external complexation of the HIC given their highly disparate sizes (>50 nm for the HIC vs. ~5 nm for the dendrimer). The zeta potential measurement of the HIC prior to incorporation with the dendrimer was found to be −9.9 mV, and this value decreased to −6.5 mV after incorporation, indicating that dendrimer complexation occurred as anticipated. To generate a calculated BRET efficiency in a biological matrix and compare it with the HIC efficiency in deep tissue imaging applications, these HIC–dendrimer complexes were used for cellular imaging on an IVIS instrument (Caliper Technologies). Images were acquired from the HIC–dendrimer complex using 660 ± 20 and 500 ± 20 nm filters (for QDs and Rluc, respectively) and demonstrated strong emissions (Fig. 5A and B) at both wavelengths, whereas the control imaging construct of bRluc–G5-PAMAM (bRluc-D) without QDSV displayed only Rluc emission (Fig. 5C and D). Based on the photon flux obtained from the control (bRluc-D) and the imaging construct (HIC dendrimer) using Living Image 4.2 software (Caliper Technologies), a preliminary BRET efficiency of approximately 72% was calculated, indicating that the HIC exceeded our expectations in a biological matrix. We believe that this improvement over the HIC alone could be due to stabilization of the HIC within the G5-PAMAM. Based on the success of our in vitro results, in vivo imaging using C57BL/6 mice was performed (Fig. 6A and B) to evaluate the imaging prospects of the HIC in live animals. For this, the HIC was encapsulated within PDD, a dendrimer complex displaying the targeting peptide (AKXVAAWTLKAAAZC), to generate an in vivo imaging complex (HIC–PDD). The dendrimer with targeting peptide was chosen for this study because it allows for specific targeting of drugs to antigen-presenting cells in the spleen. We anticipated that targeting of the HIC to a specific organ may yield better imaging output. Electrostatic encapsulation of the HIC within the PDD was achieved by incubating the two components together in a phosphate buffer (pH 7.0).

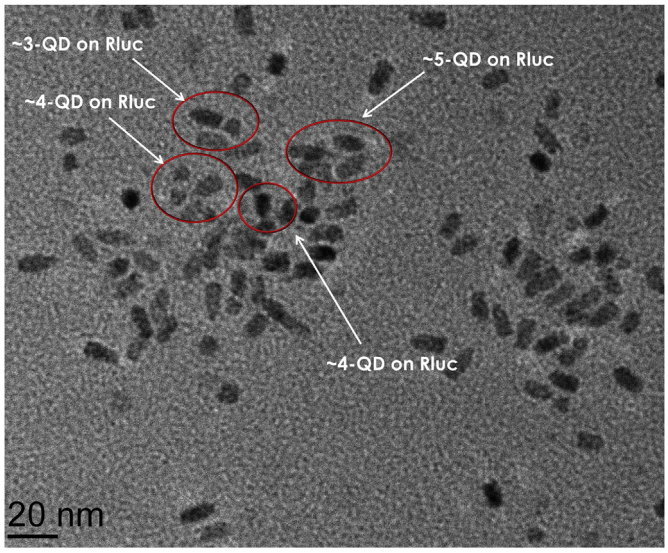

Fig.4. HR–TEM image of bRluc QDSV (HIC) complex.

For in vivo imaging, C57BL/6 mice were subcutaneously injected with approximately 0.4 μg of HIC–PDD or bRluc–PDD and images were acquired 4 h post-injection. Mice injected with HIC–PDD showed strong emissions without a filter (Fig. 6A) as well as with the 660 ± 20 nm filter (Fig. 6B) for QD emission. The bRluc–PDD complex did not show detectable bioluminescence emission (Fig. 6A and B, right mice) at similar concentrations – likely a result of biological attenuation of the Rluc signal at these low concentrations.

Recent reports [39] have demonstrated that constructs of similar size and chemistry (based on streptavidin–biotin interaction) can be used for in vitro and in vivo studies. Furthermore, in the case of HIC–PDD, energy transfer to the red-emitting QDs can overcome any issues with blue–green light absorption. As shown from the IVIS images in Fig. 6A and B, the HIC–PDD complex appears to have localized near the spleen where a high concentration of MHC class II cells is anticipated. However, the main scope of the current work was to demonstrate that the designed HIC complex can be used for in vivo and in vitro imaging applications and not necessarily targeting; therefore, further histological studies were beyond the scope of the current study.

Conclusion

In this work, we demonstrated the facile synthesis, characterization, and application of a BRET-based hybrid-imaging construct. Our studies demonstrated the formation of imaging constructs composed of a central bioluminescent donor core (bRluc) decorated with multiple acceptors (QDSV). Furthermore, the formation of these imaging constructs used reproducible self-assembly of QDSV and bRluc, successfully producing high BRET efficiency (64.8%). Finally, we were able to apply these nanostructures directly to

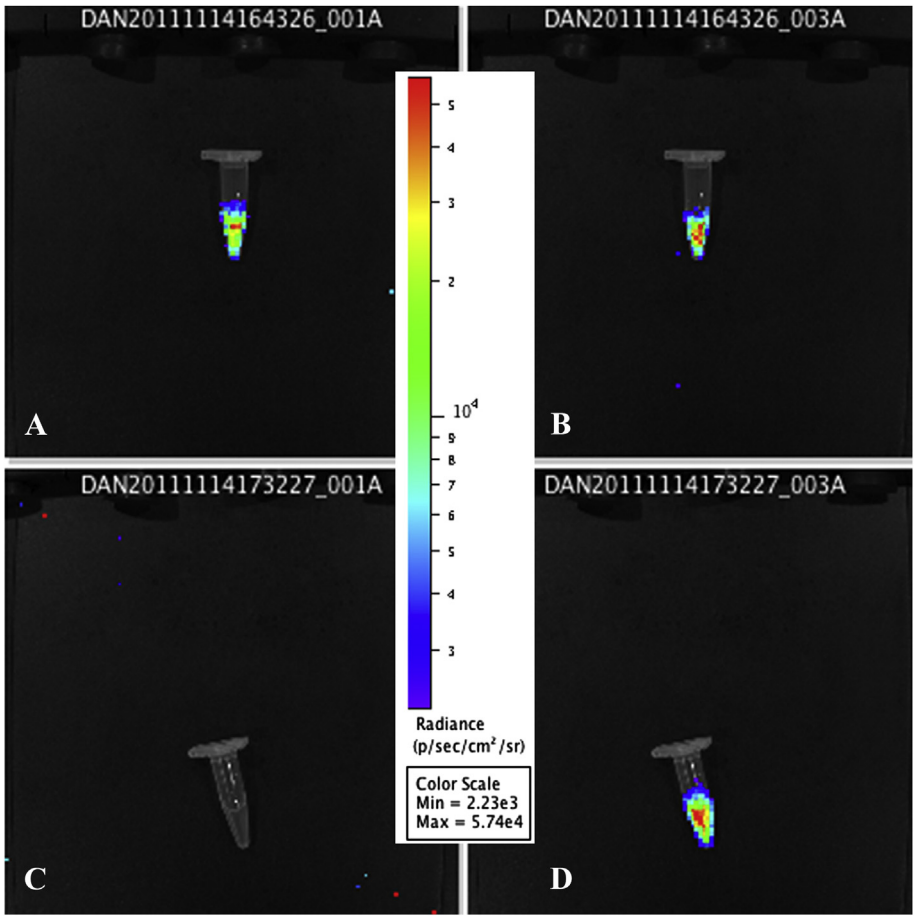

Fig.5. Self-assembled, encapsulated hybrid-imaging construct (HIC-D) transfected into ARPE-19 cells was imaged using 660 ± 20 nm (A) and 500 ± 20 nm (B) filters. Similarly, the encapsulated bRluc control (bRluc-D) was imaged using 660 ± 20 nm (C) and 500 ± 20 nm (D) filters. All images were obtained using an IVIS imaging system.

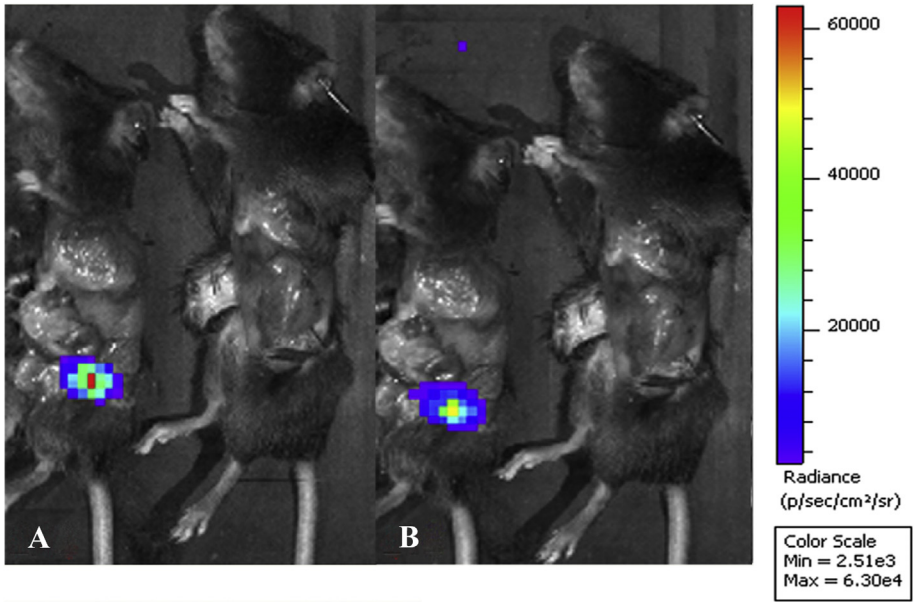

Fig.6. Imaging the HIC–PDD. The mouse on the left in each frame was injected with the targeted imaging construct HIC–PDD, whereas the mouse on the right was injected with control bRluc–PDD. Images were acquired post-subcutaneous injection of coelenterazine using no filter (A) or 660 ± 20 nm filter (B).

in vitro imaging applications while demonstrating that a recently developed encapsulation method provided for in vivo imaging.

Acknowledgments

S.K.D. thanks the National Institutes of Health (R01GM114321) and the National Science Foundation (CHE-0748648) for funding this work. S.D. thanks the National Institutes of Health (R01GM047915) for supporting this work. We also acknowledge Nicholas Chaniotakis from the University of Crete for help with obtaining HR–TEM images of the complex.

References

[1] W. Cai, X. Chen, Nanoplatforms for targeted molecular imaging in living subjects, Small 3 (2007) 1840–1854.
[2] W.C. Chan, S. Nie, Quantum dot bioconjugates for ultrasensitive nonisotopic detection, Science 281 (1998) 2016–2018.
[3] A.R. Clapp, I.L. Medintz, J.M. Mauro, B.R. Fisher, M.G. Bawendi, H. Mattoussi, Fluorescence resonance energy transfer between quantum dot donors and dye-labeled protein acceptors, J. Am. Chem. Soc. 126 (2004) 301–310.
[4] M. Kumar, D. Zhang, D. Broyles, S.K. Deo, A rapid, sensitive, and selective bioluminescence resonance energy transfer (BRET)-based nucleic acid sensing system, Biosens. Bioelectron 30 (2011) 133–139.
[5] I.L. Medintz, A.R. Clapp, H. Mattoussi, E.R. Goldman, B. Fisher, J.M. Mauro, Self-assembled nanoscale biosensors based on quantum dot FRET donors, Nat. Mater. 2 (2003) 630–638.
[6] I.L. Medintz, H.T. Uyeda, E.R. Goldman, H. Mattoussi, Quantum dot bioconjugates for imaging, labelling, and sensing, Nat. Mater. 4 (2005) 435–446.
[7] X. Gao, Y. Cui, R.M. Levenson, L.W. Chung, S. Nie, In vivo cancer targeting and imaging with semiconductor quantum dots, Nat. Biotechnol. 22 (2004) 969–976.
[8] S. Kim, Y.T. Lim, E.G. Soltesz, A.M. De Grand, J. Lee, A. Nakayama, et al., Near-infrared fluorescent type II quantum dots for sentinel lymph node mapping, Nat. Biotechnol. 22 (2004) 93–97.
[9] R.J. Macfarlane, B. Lee, M.R. Jones, N. Harris, G.C. Schatz, C.A. Mirkin, Nanoparticle superlattice engineering with DNA, Science 334 (2011) 204–208.
[10] L. Zhang, F.X. Gu, J.M. Chan, A.Z. Wang, R.S. Langer, O.C. Farokhzad, Nanoparticles in medicine: therapeutic applications and developments, Clin. Pharmacol. Ther. 83 (2008) 761–769.
[11] M. Bruchez Jr., M. Moronne, P. Gin, S. Weiss, A.P. Alivisatos, Semiconductor nanocrystals as fluorescent biological labels, Science 281 (1998) 2013–2016.
[12] D.M. Chudakov, S. Lukyanov, K.A. Lukyanov, Fluorescent proteins as a toolkit for in vivo imaging, Trends Biotechnol. 23 (2005) 605–613.
[13] X. He, J. Gao, S.S. Gambhir, Z. Cheng, Near-infrared fluorescent nanoprobes for cancer molecular imaging: status and challenges, Trends Mol. Med. 16 (2010) 574–583.
[14] X. Michalet, F.F. Pinaud, L.A. Bentolila, J.M. Tsay, S. Doose, J.J. Li, et al., Quantum dots for live cells, in vivo imaging, and diagnostics, Science 307 (2005) 538–544.
[15] B.W. Rice, M.D. Cable, M.B. Nelson, In vivo imaging of light-emitting probes, J. Biomed. Opt. 6 (2001) 432–440.
[16] Y. He, R.K. Wang, Improvement of low-level light imaging performance using optical clearing method, Biosens. Bioelectron. 20 (2004) 460–467.
[17] A.M. Loening, A.M. Wu, S.S. Gambhir, Red-shifted *Renilla reniformis* luciferase variants for imaging in living subjects, Nat. Methods 4 (2007) 641–643.
[18] H. Mattoussi, J.M. Mauro, E.R. Goldman, G.P. Anderson, V.C. Sundar, F.V. Mikulec, et al., Self-assembly of CdSe–ZnS quantum dot bioconjugates using an engineered recombinant protein, J. Am. Chem. Soc. 122 (2000) 12142–12150.
[19] C.R. Kagan, C.B. Murray, M.G. Bawendi, Long-range resonance transfer of electronic excitations in close-packed CdSe quantum-dot solids, Phys. Rev. B 54 (1996) 8633–8643.
[20] J. Du, C. Yu, D. Pan, J. Li, W. Chen, M. Yan, et al., Quantum-dot-decorated robust transductable bioluminescent nanocapsules, J. Am. Chem. Soc. 132 (2010) 12780–12781.
[21] M.K. So, C. Xu, A.M. Loening, S.S. Gambhir, J. Rao, Self-illuminating quantum dot conjugates for in vivo imaging, Nat. Biotechnol. 24 (2006) 339–343.
[22] Z. Xia, J. Rao, Biosensing and imaging based on bioluminescence resonance energy transfer, Curr. Opin. Biotechnol. 20 (2009) 37–44.
[23] Y. Xu, D.W. Piston, C.H. Johnson, A bioluminescence resonance energy transfer (BRET) system: application to interacting circadian clock proteins, Proc. Natl. Acad. Sci. USA 96 (1999) 151–156.
[24] V. Sholin, J.D. Olson, S.A. Carter, Semiconducting polymers and quantum dots in luminescent solar concentrators for solar energy harvesting, J. Appl. Phys. 101 (2007) 123114.
[25] A. Roda, M. Guardigli, E. Michelini, M. Mirasoli, Bioluminescence in analytical chemistry and in vivo imaging, Trends Anal. Chem. 28 (2009) 307–322.
[26] J.K. Jaiswal, S.M. Simon, Potentials and pitfalls of fluorescent quantum dots for biological imaging, Trends Cell Biol. 14 (2004) 497–504.
[27] K.A. Cissell, S. Campbell, S.K. Deo, Rapid, single-step nucleic acid detection, Anal. Bioanal. Chem. 391 (2008) 2577–2581.
[28] W.R. Algar, M.G. Ancona, A.P. Malanoski, K. Susumu, I.L. Medintz, Assembly of a concentric Forster resonance energy transfer relay on a quantum dot scaffold: characterization and application to multiplexed protease sensing, ACS Nano 6 (2012) 11044–11058.
[29] W.R. Algar, D. Wegner, A.L. Huston, J.B. Blanco-Canosa, M.H. Stewart, A. Armstrong, et al., Quantum dots as simultaneous acceptors and donors in time-gated Forster resonance energy transfer relays: characterization and biosensing, J. Am. Chem. Soc. 134 (2012) 1876–1891.
[30] A.I. Fabian, T. Rente, J. Szollosi, L. Matyus, A. Jenei, Strength in numbers: effects of acceptor abundance on FRET efficiency, ChemPhysChem 11 (2010) 3713–3721.
[31] S.V. Koushik, P.S. Blank, S.S. Vogel, Anomalous surplus energy transfer observed with multiple FRET acceptors, PLoS One 4 (11) (2009) e8031.
[32] J.R. Lakowicz, Principles of Fluorescence Spectroscopy, third ed., Springer, New York, 2006.
[33] C.A. Leatherdale, W.K. Woo, F.V. Mikulec, M.G. Bawendi, On the absorption cross section of CdSe nanocrystal quantum dots, J. Phys. Chem. B 106 (2002) 7619–7622.
[34] P. Daftarian, A.E. Kaifer, W. Li, B.B. Blomberg, D. Frasca, F. Roth, et al., Peptide-conjugated PAMAM dendrimer as a universal DNA vaccine platform to target antigen-presenting cells, Cancer Res. 71 (2011) 7452–7462.
[35] A.M. Loening, T.D. Fenn, S.S. Gambhir, Crystal structures of the luciferase and green fluorescent protein from *Renilla reniformis*, J. Mol. Biol. 374 (2007) 1017–1028.
[36] J.C. Matthews, K. Hori, M.J. Cormier, Substrate and substrate analogue binding properties of *Renilla* luciferase, Biochemistry 16 (1977) 5217–5220.
[37] J.C. Matthews, K. Hori, M.J. Cormier, Purification and properties of *Renilla reniformis* luciferase, Biochemistry 16 (1977) 85–91.
[38] K.C. Dunn, A.E. Aotaki-Keen, F.R. Putkey, L.M. Hjelmeland, ARPE-19, a human retinal pigment epithelial cell line with differentiated properties, Exp. Eye Res. 62 (1996) 155–169.
[39] D. Sen, T.J. Deerinck, M.H. Ellisman, I. Parker, M.D. Cahalan, Quantum dots for tracking dendritic cells and priming an immune response in vitro and in vivo, PLoS One 3 (9) (2008) e3290.